GEOMETRIC AND AERODYNAMIC ROUGHNESS OF SEA ICE

S. MAI[1], C. WAMSER[1], C. KOTTMEIER[1,2]
[1] Alfred Wegener Institut for Polar and Marine Research, Bremerhaven, Germany
[2] Institut für Umweltphysik, Universität Bremen, Bremen, Germany

Abstract. The aerodynamic drag of Arctic sea ice is calculated using surface data, measured by an airborne laser altimeter and a digital camera in the marginal ice zone of Fram Strait. The influence of the surface morphology on the momentum transfer under neutral thermal stratification in the atmospheric boundary layer is derived with the aid of model concepts, based on the partitioning of the surface drag into a form drag and a skin drag. The drag partitioning concept pays attention to the probability density functions of the geometric surface parameters. We found for the marginal ice zone that the form drag, caused by floe edges, can amount to 140% of the skin drag, while the effect of pressure ridges never exceeded 40%. Due to the narrow spacing of obstacles, the skin drag is significantly reduced by the shadowing effects on the leeward side of floe edges. For practical purposes, the fractional sea-ice coverage can be used to parameterize the drag coefficient C_{dn}, related to the 10m-wind. C_{dn} increases from $1.2 \cdot 10^{-3}$ over open water to $2.8 \cdot 10^{-3}$ for 55% ice coverage and decreases to $1.5 \cdot 10^{-3}$ for 100% ice coverage.

Aircraft turbulence measurements are used to compare the model values of C_{dn} with measurements. The correlation between measured and modelled drag coefficients result in $r^2 = 0.91$, where r is the correlation coefficient.

Symbols

$C_{dn(z)}$	neutral drag coefficient at height z
C	ice concentration
d_f	distance of ice floes
d_r	distance of pressure ridges
$d_{r,min}$	threshold of pressure ridge distance
$\vec{F}$	form drag
$\vec{F}_f$	form drag of ice floe edges
$\vec{F}_r$	form drag of pressure ridges
h_f	height of ice floes
h_r	height of pressure ridges
$h_{r,min}$	threshold of pressure ridge height
l_f	length of ice floes
m	parameter specifying the obstacle shadowing effect
$p_{(h_f,l_f,d_f)}$	probability density function of floe parameters
$p_{(h_r,d_r)}$	probability density function of pressure ridge parameters
$\vec{S}$	skin drag
$\vec{S}_{w0}$	skin drag of an ice free water surface
$\vec{S}_{i0}$	skin drag of a closed ice cover without pressure ridges

u_{*i}	friction velocity over ice
u_{*w}	friction velocity over water
$\vec{V}_{(z)}$	wind velocity
Z_2	matching height
z_{0eff}	effective roughness length
z_{0i}	local roughness length of sea ice
z_{0w}	local roughness length of water
α_f	form drag parameter of ice floes
α_r	form drag parameter of pressure ridges
κ	von Karman constant
λ_j	fitting parameters for pressure ridges
μ_j	fitting parameters for ice floes
ρ	air density
$\vec{\tau}$	total surface drag

1. Introduction

The ice cover of the Arctic Ocean is characterized by significant spatial and temporal variability. The predominant annual period, during which the ice extent ranges from 8 million km² in late summer to 15 million km² in late winter (see e.g. Gloersen and Campbell, 1988), is primarily caused by freezing and melting processes. Shorter fluctuations are also affected by dynamic forces exerted by surface winds and ocean currents. These influences depend critically on the morphology at the top and bottom of the sea ice cover. These geometric structures affect the exchange of heat and momentum between the atmosphere and the sea ice as well as between the ocean and the sea ice (Wefelmeier and Etling, 1991). Formally the surface influence on the turbulent momentum flux is expressed through drag coeficients or the aerodynamic roughness length of sea ice. Overland (1985) proposes an effective roughness length z_{0eff} in the framework of similarity theory, which accounts for different types of surfaces. Banke *et al.* (1973) parameterize z_{0eff} by the standard deviation of the geometric surface height of the partly ice covered ocean. Arya (1975) partitions the total surface drag acting on a sea-ice cover into two components, the form and the skin drag. Joffre (1983) and Dierking (1995) apply this concept to closed pack-ice fields. Hanssen-Bauer and Gjessing (1988) (subsequently:HBG) consider the effects of floe edges of broken ice-fields, but they neglect the form drag of pressure ridges. Hartmann *et al.* (1994) find from aircraft gust probe measurements that the form drag of sea-ice surfaces increases linearly with the ice-area perpendicular to the wind vector. Our study aims to determine an optimized drag partitioning model on the basis of adequate surface information and aircraft turbulence data. The models of Arya (1975) and HBG were combined. Probability functions of the surface parameters height, distance and width of ice floes and ridges were determined and introduced in our model.

2. Morphological Surface Parameters Controlling the Aerodynamic Drag of Sea Ice

The stress exerted on a partly ice covered sea surface by the surface wind field depends on the hydrodynamic roughness of the flat water and sea-ice surfaces (skin drag) and on the resistance of larger obstacles like the floe edges and the pressure ridges (form drag). According to the drag partitioning concept the total surface drag $\vec{\tau}$ can be expressed as the sum of form drag $\vec{F}$ and skin drag $\vec{S}$:

$$\vec{\tau} = \vec{F} + \vec{S} \tag{1}$$

While the model of Arya (1975) accounts for the effects of ridges on the form drag, Hanssen-Bauer and Gjessing (1988)[HBG] treat the influence of floe edges on the surface momentum exchange. The relative values $|\vec{F}|/|\vec{S}_{w0}|$, $|\vec{S}|/|\vec{S}_{w0}|$ and $|\vec{\tau}|/|\vec{S}_{w0}|$ of the form drag, the skin drag and the total drag respectively normalized by the drag of a water surface $|\vec{S}_{w0}|$ can be determined from these models.
We combine the models of HBG and Arya but apply probability density functions of the roughness parameters instead of mean quantities in the model equations. The total form drag $\vec{F}$ thus results in a combination of the floe edge component $\vec{F}_f$ and the ice-ridge component $\vec{F}_r$ as

$$\frac{|\vec{F}|}{|\vec{S}_{w0}|} = \frac{|\vec{F}_r|}{|\vec{S}_{w0}|} + C\frac{|\vec{F}_r|}{|\vec{S}_{i0}|}\frac{|\vec{S}_{i0}|}{|\vec{S}_{w0}|}. \tag{2}$$

The ratio of the skin drag of ice surfaces $\vec{S}_{i0}$ and water surfaces $\vec{S}_{w0}$ can be expressed by application of logarithmic wind profiles over ice with roughness z_{0i} and water with roughness z_{0w} as

$$\frac{|\vec{S}_{i0}|}{|\vec{S}_{w0}|} = \left(\frac{ln\,(Z_2 / z_{0w})}{ln\,(Z_2 / z_{0i})}\right)^2, \tag{3}$$

where Z_2 is the matching height of the wind, assumed to be constant (20m) for the ice conditions under consideration. This and the following equations refer to near neutral stratification; non-neutral cases are not considered. The ridge form drag $\vec{F}_r$ is weighted by the ice concentration C, since the number of ridges per unit area depends on the ice concentration.

With the aid of probability density functions $p_{(h_f, l_f, d_f)}$, which determine the density of unit area of special parameter combinations, the ratios $|\vec{F}_r|/|\vec{S}_{w0}|$ and $|\vec{S}|/|\vec{S}_{w0}|$ result as

$$\frac{|\vec{F}|}{|\vec{S}_{w0}|} = \int_0^\infty \int_0^\infty \int_0^\infty p_{(h_f, l_f, d_f)} \frac{|\vec{F}_{f(h_f, l_f, d_f)}|}{|\vec{S}_{w0}|} dh_f\, dl_f\, d(d_f), \tag{4}$$

$$\frac{|\vec{S}|}{|\vec{S}_{w0}|} = \int_0^\infty \int_0^\infty \int_0^\infty p_{(h_f, l_f, d_f)} \frac{|\vec{S}_{f(h_f, l_f, d_f)}|}{|\vec{S}_{w0}|} dh_f\, dl_f\, d(d_f), \tag{5}$$

$$\frac{|\vec{\tau}|}{|\vec{S}_{w0}|} = \frac{|\vec{F}_f|}{|\vec{S}_{w0}|} + \frac{|\vec{S}|}{|\vec{S}_{w0}|}, \tag{6}$$

with

$$\frac{|\vec{F}_{f(h_f,l_f,d_f)}|}{|\vec{S}_{w0}|}=\frac{\alpha f}{\kappa^2}\frac{h_f}{l_f+d_f}\left(\ln\left(\frac{h_f}{z_{0w}\cdot e}\right)\left(1-\exp\left(-0.18\frac{d_f}{h_f}\right)\right)\right)^2, \tag{7}$$

$$\frac{|\vec{S}_{(h_f,l_f,d_f)}|}{|\vec{S}_{w0}|}=\begin{cases}1+\dfrac{l_f}{l_f+d_f}\left(\left(\dfrac{ln\left(\frac{Z_2}{z_{0w}}\right)}{ln\left(\frac{Z_2}{z_{0i}}\right)}\right)^2-1-m\dfrac{h_f}{l_f}\right), & \dfrac{d_f}{h_f}>m\\ \dfrac{l_f}{l_f+d_f}\left(\dfrac{ln\left(\frac{Z_2}{z_{0w}}\right)}{ln\left(\frac{Z_2}{z_{0i}}\right)}\right)^2, & \dfrac{d_f}{h_f}\le m.\end{cases} \tag{8}$$

In these equations the floes are characterised by their lengths l_f, their edge heights h_f, their spacings d_f and the edge form drag parameter α_f. In the following the ridges are analogously characterised by their heights h_r, their spacings d_r and the ridge form drag parameter α_r. κ is the von Karman constant and m is a parameter specifying the leeward extent $x = m\ h_{f,r}$ of obstacle shadowing, i.e. reduction of the surface stress in the leeward side of an obstacle. In this study we use m = 20 (see Plate and Lin, 1965) and $\alpha_f = 0.5$ (see Marshall, 1971). The small-scale roughness lengths are prescribed as $z_{0w} = 0.00012$ m for water (see Large and Pond, 1981) and $z_{0i} = 0.00025$ m for ice, based on numerous studies for level ice (Banke and Smith,1973).

In the HBG model, the integrals of Equations (4) and (5) are replaced by mean values. Also the reduction of the skin drag of the ice surface, due to the shadowing of ridges, is disregarded. To obtain an improved formulation, the skin drag is expressed by

$$|\vec{S}_i|=\frac{|\vec{S}_i|}{|\vec{S}_{i0}|}\rho u_{*i}^2 \tag{9}$$

where the ratio $|\vec{S}_i|/|\vec{S}_{i0}|$ is identical to (12).

In our approach the expression $\dfrac{|\vec{S}_{(h_f,l_f,d_f)}|}{|\vec{S}_{w0}|}$ in Equation (5) reads

$$\frac{|\vec{S}_{(h_f,l_f,d_f)}|}{|\vec{S}_{w0}|}=\begin{cases}1+\dfrac{l_f}{l_f+d_f}\left(\left(\dfrac{ln\left(\frac{Z_2}{z_{0w}}\right)}{ln\left(\frac{Z_2}{z_{0i}}\right)}\right)^2\dfrac{|\vec{S}_i|}{|\vec{S}_{i0}|}-1-m\dfrac{h_f}{l_f}\right), & \dfrac{d_f}{h_f}>m\\ \dfrac{l_f}{l_f+d_f}\left(\dfrac{ln\left(\frac{Z_2}{z_{0w}}\right)}{ln\left(\frac{Z_2}{z_{0i}}\right)}\right)^2\dfrac{|S_i|}{|\vec{S}_{i0}|}, & \dfrac{d_f}{h_f}\le m.\end{cases} \tag{10}$$

Arya´s model (1973, 1975) for the influence of ice ridges on the atmospheric flow is modified by applying the probability density function $p_{(h_r,d_r)}$ instead of mean ridge spacing. Thus the ratios $|\vec{F}_r|/|\vec{S}_{i0}|$ and $|\vec{S}_i|/|\vec{S}_{i0}|$ are

$$\frac{|\vec{F}_r|}{|\vec{S}_{i0}|} = \frac{1}{\pi\kappa^2}\int_0^{\infty}\int_{h_{r,\min}}^{\infty}\alpha_r\left(\ln\left(\frac{h_r}{z_{0i}}\right)\left(1-\exp\left(-0.18\frac{h_r}{d_r}\right)\right)\right)^2\frac{h_r}{d_r}\,p_{(h_r,d_r)}\,dh_r\,d(d_r) \tag{11}$$

$$\frac{|\vec{S}_i|}{|\vec{S}_{i0}|} = \int_0^{\infty}\int_{h_{r,\min}}^{\infty}\frac{|\vec{S}_{r(h_r,d_r)}|}{|\vec{S}_{i0}|}\frac{h_r}{d_r}\,p_{(h_r,d_r)}\,dh_r\,d(d_r), \tag{12}$$

with

$$\frac{|\vec{S}_{r(h_r,d_r)}|}{|\vec{S}_{i0}|} = \begin{cases}\left(1-m\dfrac{h_r}{d_r}\right), & \dfrac{h_r}{d_r} > m\\ 0, & \dfrac{h_r}{d_r} \le m.\end{cases} \tag{13}$$

The drag coefficient $C_{dn(z)}$ results from

$$C_{dn(z)} = \frac{|\vec{\tau}|}{|\vec{S}_{w0}|}\cdot\frac{|\vec{S}_{w0}|}{\rho\bar{\vec{v}}^2_{(z)}} \tag{14}$$

where the surface drag of water surface is $|\vec{S}_{w0}| = \rho u_{*w}^2$. By application of a logarithmic wind profile over water $\bar{\vec{v}}_{(z)} \approx \frac{u_{*w}}{\kappa}\,ln\left(\frac{z}{z_{0w}}\right)$ the neutral drag coefficient results as

$$C_{dn(z)} = \frac{|\vec{\tau}|}{|\vec{S}_{w0}|}\frac{\kappa^2}{\left(\ln\left(\frac{z}{z_{0w}}\right)\right)^2}. \tag{15}$$

3. Surface Roughness Parameters in the Marginal Ice Zone of Fram Strait

Information on floe size, freeboard height and spacing of ice ridges as well as turbulent fluxes of heat, humidity and momentum are obtained from airborne surveys during the experiment REFLEX II (Radiation and Eddy Flux Experiment). The measurements were carried out in late winter over the pack-ice region north and west of Svalbard in February and March, 1993. REFLEX II (Kottmeier *et al*., 1994 and Mai, 1995) was an observational programme studying atmospheric processes affected by the presence of sea ice in wintertime. The programme´s objectives comprised the effects of low level – mainly stratiform – clouds on the vertical radiative fluxes, the measurement of surface data as ground truth for satellite remote sensing of sea ice and the acquisition of data for the forcing and validation of mesoscale atmospheric models. A central objective of the programme is to derive schemes which parameterize turbulent fluxes in relation to sea-ice statistics, since the vertical exchange of momentum and energy vary considerably with ice concentration, ice thickness and floe size distribution. The turbulent fluxes of heat,

humidity and momentum are determined from data obtained with the *Meteopod* turbulence probing system, which is mounted under the right wing of Dornier DO-228 turbo-prop aircraft. Information on surface structure is obtained by means of a laser altimeter and downward looking line-scan cameras. The Dornier DO-228 (Polar 2) aircraft is equipped corresponding to IFR (instrumental flight rules) and has a laser-gyro inertial navigation system (INS). In addition a separate global positioning system (GPS) is available for precise-navigation. Low level horizontal flight legs cover distances of 20 to 50 km in the sea-ice region and are organized for a wide range of ice concentrations and thermal stratifications. They are repeated several times in order to obtain reliable turbulence statistics. During REFLEX II the research vessel POLARSTERN was in the sea ice. Therefore it was possible to fly several sections for the intercomparison of aircraft and ground data. Aircraft turbulence data at level between 30 m and 40 m are available for total flight lengths of 2970 km,

POLAR 2 carries a downward looking laser altimeter in order to resolve the topographic structures of the surface down to a centimeter scale. The distance is determined from the reflection of the laser pulse from the surface. The reflectivity of water is too small for reliable measurements, but ice floes regularly provide satisfactory signals. Due to the very low air temperatures in winter leads are mostly frozen over, so that this level can also be detected by the laser altimetry. The motion of the aircraft has to be eliminated by a special method which is not described in this framework but is comprehensively discussed in Mai (1995). Technical data of the laser system are summarized in Table I.

Two digital line-scan cameras detect the intensity of visible (LSC) and the infrared (IRLS) signals of the Earth´s surface, scanning perpendicular to the flight track. They are used for floe edge detection and provide information on the ice concentration, as well as floe size distribution.

The width and cross-track resolution of the images depend on the altitude of the aircraft while the along-track resolution is determined by the aircraft´s ground speed, which is typically 70 ms^{-1}. Table II indicates some technical information on the two line-scan cameras. The cameras and observational procedures of the laser altimeter and the digital cameras and the derived quantities are displayed schematically in Figure 1.

Examples of observed quantities are presented in Figure 2. The upper two graphs show the surface height (m) and the intensity of the backscatter signal from the laser altimeter which are distinctly correlated. The LSC diode viewing exactly vertically downward still discriminates ice and leads although the along track resolution is much lower than that of the laser. In contrast the surface radiation thermometer KT4 is not sufficient to resolve leads of a few meters width.

TABLE I

Technical specifications of the laser altimeter

Type :	PS 100E, IBEO, Hamburg
Power :	100 W
Range :	100 m
Lens diameter :	42 mm
Beam divergence :	0.24°
Footprint radius :	6.3 cm (at *hf* = 30 m)
Pulse frequency :	ca. 2000 Hz
Horizontal resolution :	3.25 cm (for *vf* = 65 m s-1)
Pulse duration :	10 ns
Wavelength :	905 nm
Necessary minimum	
Backscatter intensity :	40 of 256 (arb. Units)
Distance accuracy :	3 cm (single mesurement)

TABLE II

Technical specifications of the line scan cameras

Camera system	LSC	IRLS
Sensor :	CCD 512 pixels	single IR sensor at 77 K
Spectral range :	0.4 mm to 1.1 mm	8.0 mm to 12.0 mm
Optical system :	8 mm lens, f / 1.4	rotating mirror, f / 1.1
Scan angle :	90°	90°
Cross track resolution :	12 cm (h_f = 30 m)	12 cm (h_f = 30 m)
Sampling frequency :	50Hz	50Hz
Along track resolution :	1.3 m (v_f = 65 m s-1)	1.3 m (v_f = 65 m s-1)
Sensitivity :	256 grey levels	0.1 K

The low level flights at altitudes between 30 m and 40 m are subdivided into sections of 12 km length. About 100 of those sections are the basis of the calculation of the normalized frequency distributions of l_f, d_f and h_f in order to derive the surface drag values. Examples for the pack-ice region within about 20 km distance from the ice edge are shown in Figure 3a-c together with the model functions, which are exponential for l_f, hyperbolic for d_f and form a Poisson distribution for h_f. The best fit was achieved by

$$p_{(l_f)} = -\mu_1 \exp(-\mu_1 (l_f - l_{f,\min})) \tag{16}$$

$$p_{(d_f)} = p_0 \cdot l_s^{-\mu_2} \quad , \tag{17}$$

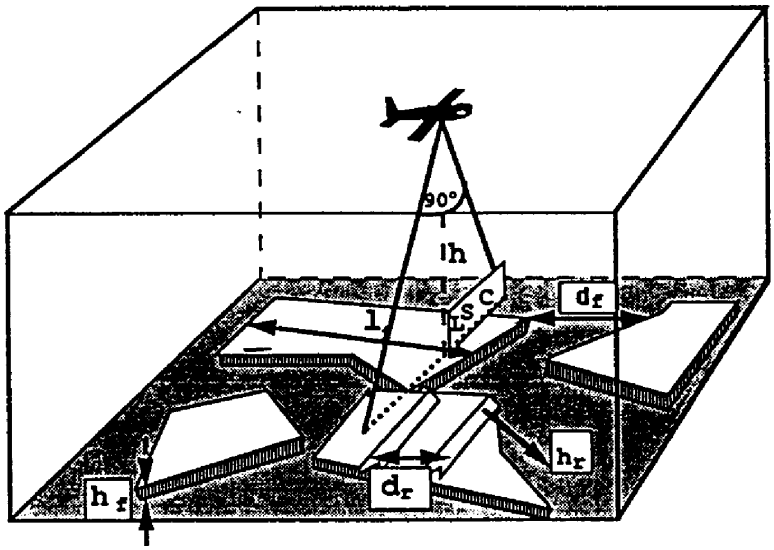

Figure 1. Geometrical parameters of ice fields, measured from aircraft. The following abbreviations are used in the text and the equations. l_f : length of the ice floe secant, h_f : free-board height, d_f : distance between the floes; h_r : height of ice ridges and d_r : distance between them.

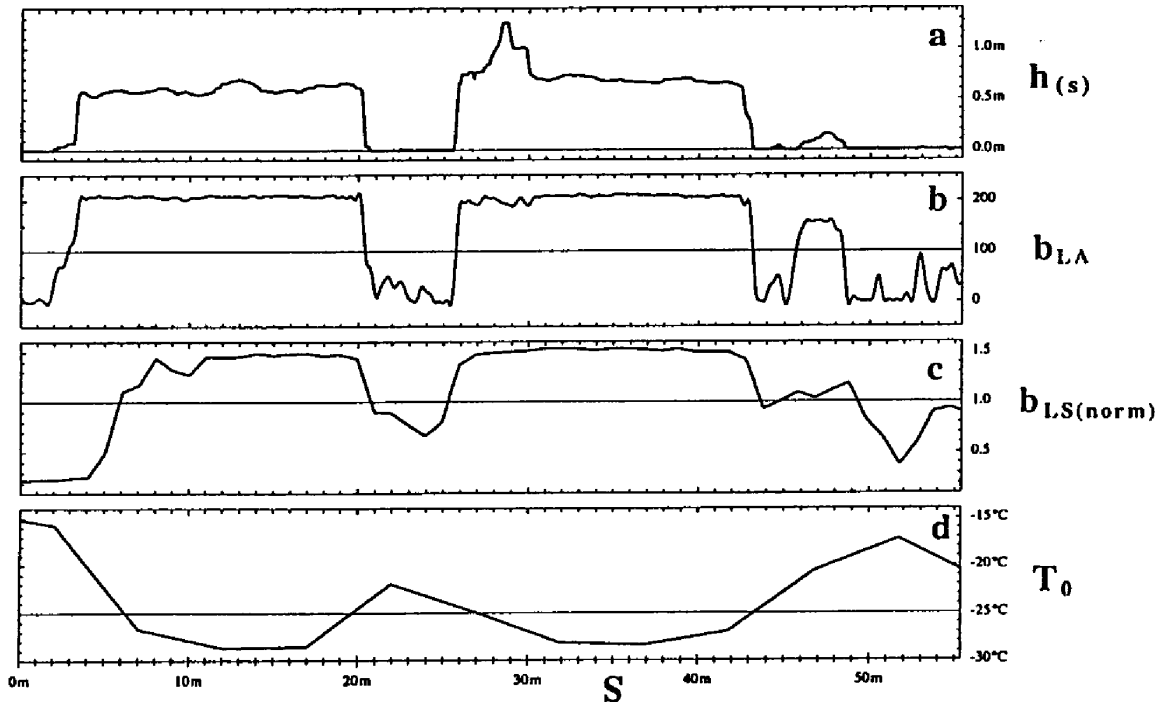

Figure 2. An example for the application of different aircraft sensors for the ice floe detection; a: surface height from the laser altimeter, corrected for the aircraft motion, b: laser echo strength, c: line averaged surface reflectivity (relative units) from line-scan camera, d: surface radiation temperature from KT4.

$$p_{(h_f)} = \frac{\mu_{3a}^{(\mu 3b+1)} h_f^{\mu 3b}}{\Gamma_{(\mu 3b+1)}} \exp\left(-\mu_{3a} h_f\right), \tag{18}$$

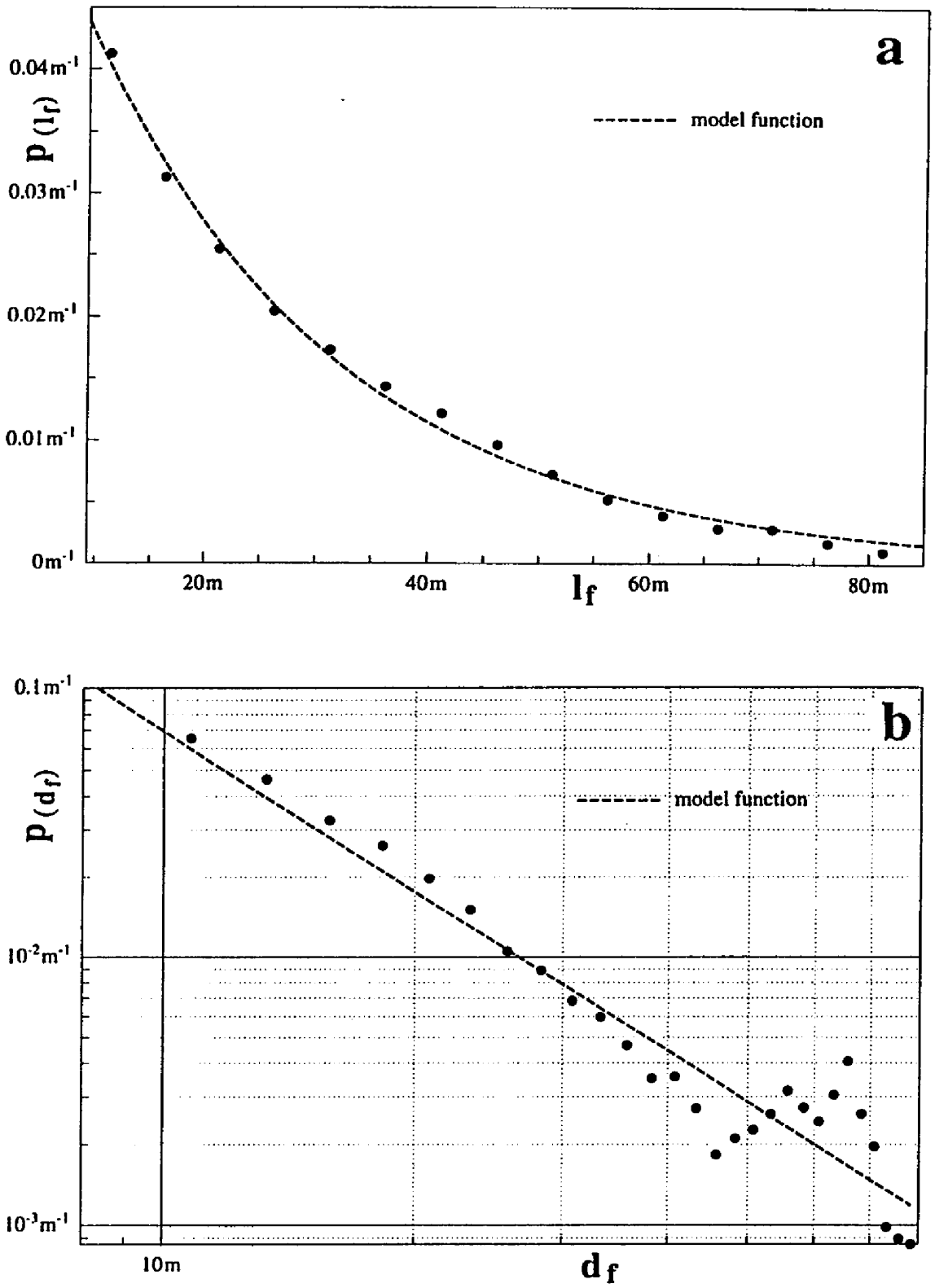

Figure 3. Normalized frequency distributions for l_f, d_f and h_f. The curves through the data points are determined by a least squares method, the corresponding correlation coefficients are $r(a) = 0.97$, $r(b) = 0.95$ and $r(c) = 0.96$.

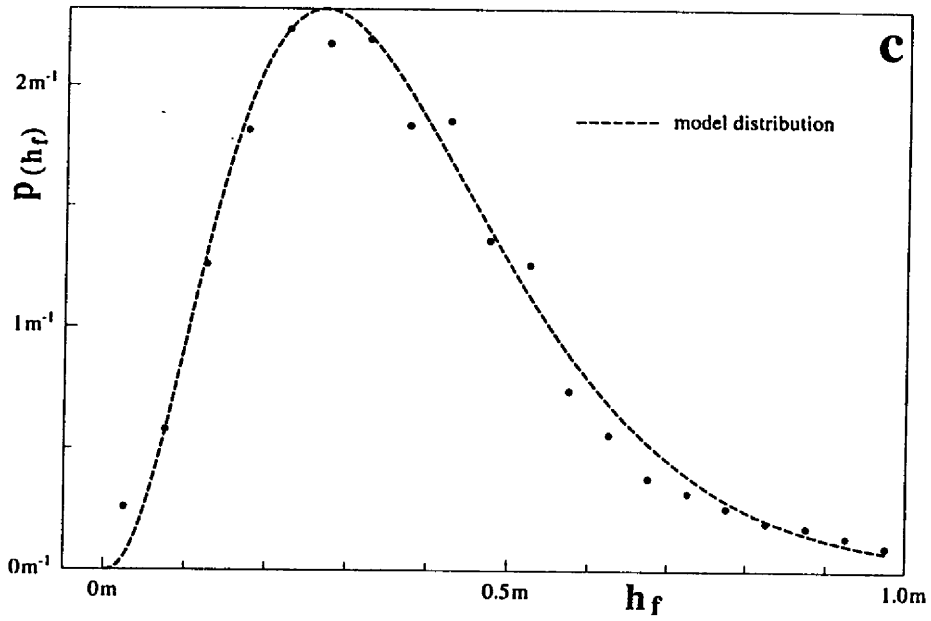

Figure 3c.

TABLE III

Summary of the investigation of ice floe parameters.

Quantity	Conditional frequency* (cf)
l_f	92%
d_f	85%
h_f	90%
h_r	98%
d_r	85%

$$\Gamma_{(\mu 3b+1)} = \int_0^\infty x^{\mu 3b} \exp(-x)dx \tag{19}$$

Similar functions were calculated for the height and the spacing of ice ridges. An example for this investigation, which refers to the same location as the previous figure, is portrayed in Figure 4a,b. The curves were obtained by a model developed by Wadhams and Davy (1986). They postulate a linear dependence between the cross-sectional area and the height of the ice ridges. Their probability density functions are

$$p_{(h_r)} = \lambda_1 e^{-\lambda_1 (h_r - h_{r,\min})} \tag{20}$$

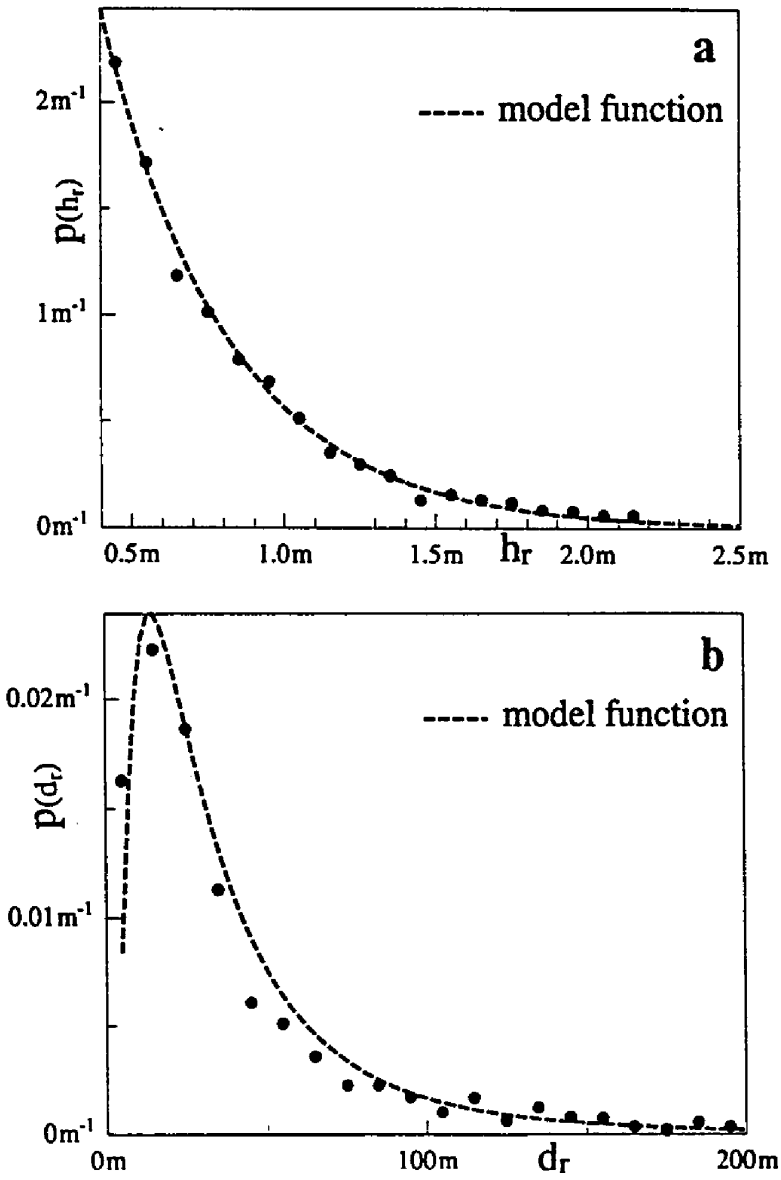

Figure 4. Normalized distributions of the heights (4a) and the distances (4b) of ice ridges. The curves through the data points correspond to Wadhams and Davy (1986). The correlation coefficients are 0.997 and 0.950, respectively.

$$p_{(d_r)} = \frac{1}{\sqrt{2\pi}\lambda_{2b}(d_r - d_{r,\min})} \exp\left(-\frac{\left(\ln\left(d_r - d_{r,\min}\right) - \lambda_{2a}\right)^2}{2\lambda_{2b}^2} \right), \tag{21}$$

where the threshold values are $h_{r,min}$ = 0.4 m and $d_{r,min}$ = 7 m. The coefficients λ_i in the Equations (20) and (21) are determined by a least squares fit of the functions $p_{(hr)}$ and $p_{(dr)}$ to the data.

Normalized frequency distributions of ridge and floe statistics for all flight legs are given in Table III. The conditional frequency, based on all flight legs of a length of 12 km, refers to correlation coefficients exceeding the value of 0.95. Obviously the empirical probability density functions generally provide suitable approximations of the observed data.

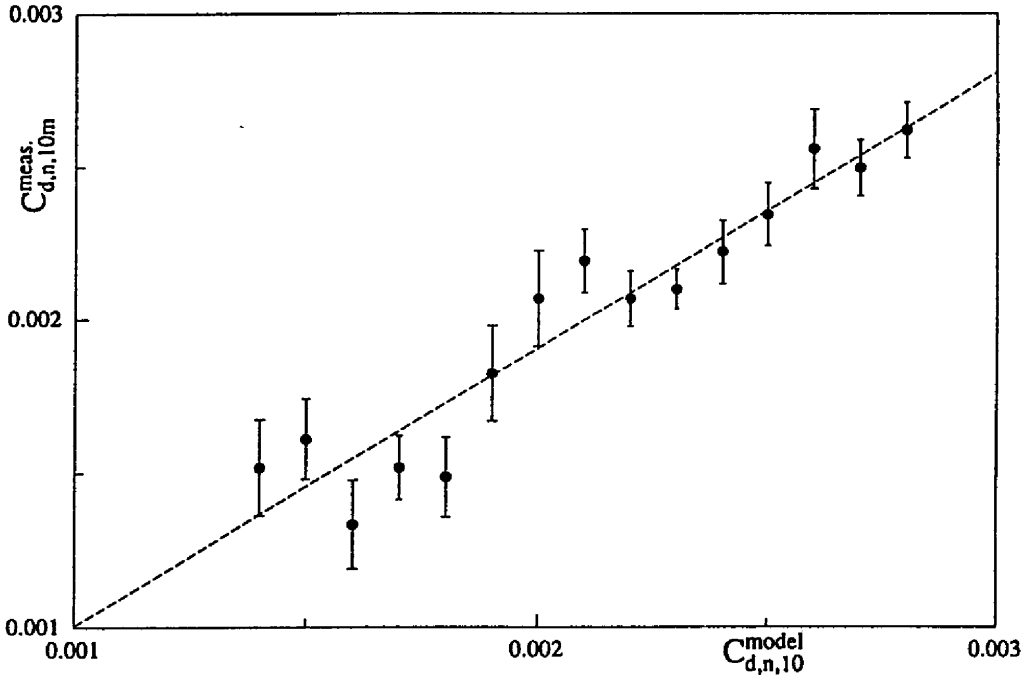

Figure 5. Drag coefficients C_{dn}^{meas} from turbulence measurements and modelled C_{dn}^{mod} considering the distribution functions of the separation and height of ice edges and ridges.

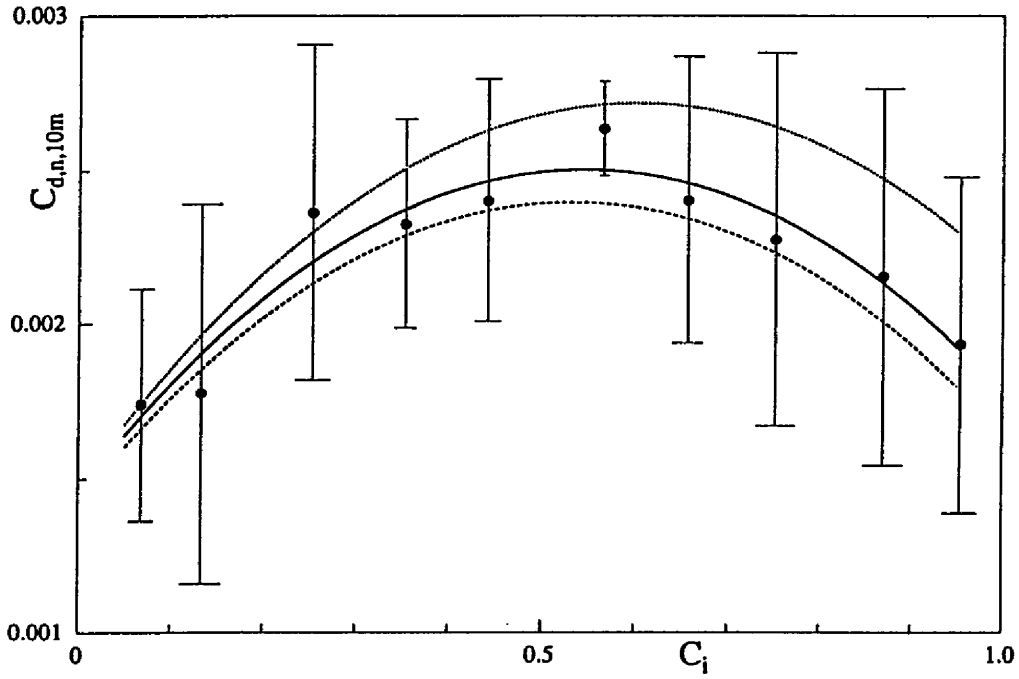

Figure 6. The neutral drag coefficient as a function of the ice concentration modelled under consideration of the form drag of floe edges and pressure ridges (solid curve), under consideration of the form drag of floe edges only (dashed). The dotted curve considers the form drag of floe edge and ridges but neglects the reduction of surface drag due to shadowing effects.

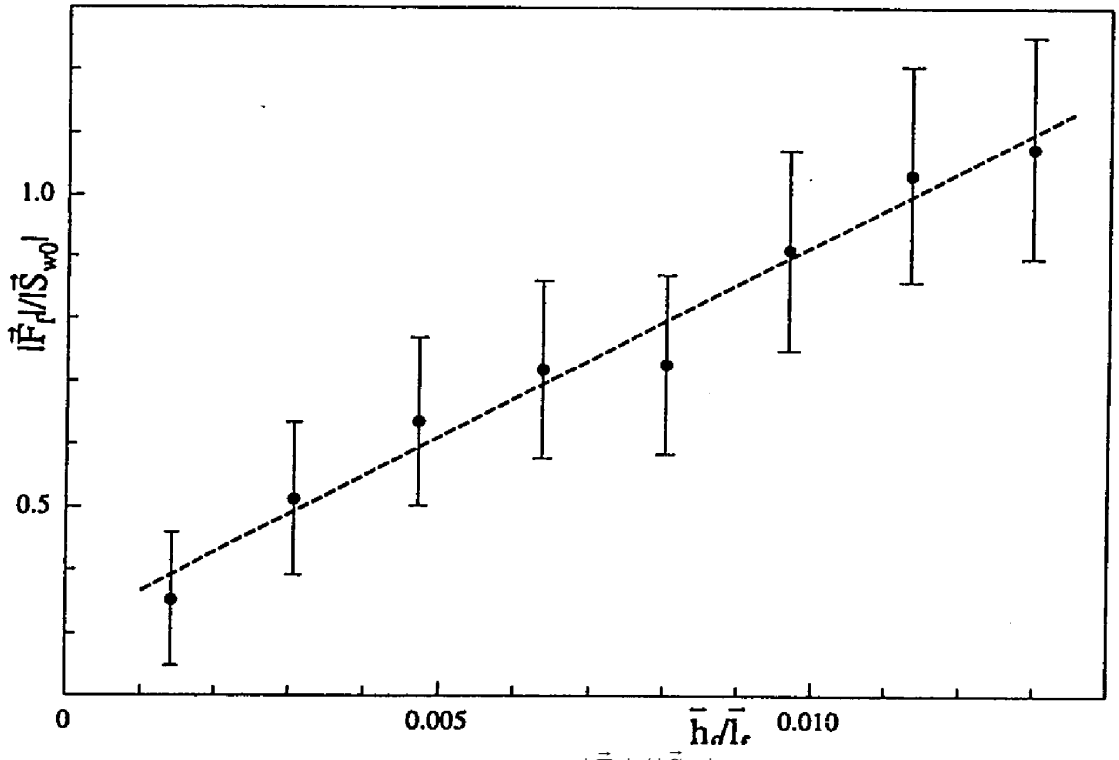

Figure 7. Regression of $|\vec{F}_f| / |\vec{S}_{w0}|$ on h_f / l_f.

4. Theoretical Drag Formulations Compared with Aircraft Turbulence Data

The model computations on the basis of geometric surface morphology and the aircraft turbulence measurements as described in section 2 are used to parameterize the aerodynamic surface drag in the Arctic marginal ice zone. Drag coefficients C_d are determined from the aircraft measurements of the mean wind vector and the eddy correlation stresses at flight levels between 30 and 40 m. These values are used for a comparison with our model values. The aircraft data are reduced to a 10 m level and to neutral density stratification with the aid of a one-dimensional numeric model. The model (Raasch, 1988; Hartmann *et al.*, 1994) uses Monin-Obukhov similarity in the surface layer, and at higher levels eddy diffusivities calculated by a Prandtl-Kolmogorov approach as a function of turbulent kinetic energy. After initialisation with steady-state wind profiles and neutral stratification up to a height of 200 m and using the measured temperature profile above, the surface temperature is adapted to the measured KT4-value. The model is run for roughly two hours to achieve nearly stationary conditions. Then the vertical profiles of temperature and wind are found to match the observed profiles reasonable well and the turbulent fluxes and the turbulent kinetic energy at flight level agree with the measurements. We therefore use the model ratio $C_{d(z)}$ to $C_{dn,10m}$ to reduce the drag coefficient derived from observations at flight level to 10m. Cases with a stably stratified atmospheric surface layer and with rather inhomogeneous ice distributions along the 12 km flight leg are eliminated. A total of 85 flight legs are accepted for comparison. The measured drag coefficients are classified according to the model result. The result is displayed in Figure 5. The model drag coefficients account for the freeboard and the pressure ridge effects. The squared correlation coefficient amounts to 0.91, whilst the slope of the regression line is also 0.91.

From the regression in Figure 5 we find that the model drag coefficients are about 10% greater then the measured ones. Reasons for this systematic difference may be caused by the reduction procedures of the measurements as well as by the model concept. Measurements planned with a helicopter-borne turbulence probe which can be exposed near the 10 m level may help to exclude observational deficits. In spite of the above mentioned uncertainties the drag formulation, based on the detailed floe edge and ridge statistics, provides a sufficient scheme for the momentum exchange at a partly ice covered sea surface.

For practical applications, e.g. in general circulation or sea-ice-models, one normally lacks detailed sea-ice information. Therefore we empirically relate our drag coefficients to the sea-ice concentration, which is principally available from satellite observations or model calculations. The result is shown in Figure 6.

The error bars indicate the variations of the drag coefficients for 10 different classes of ice concentrations due to the varying configuration of ice floes and pressure ridges. The drag coefficients for open water and for total ice cover are about 0.0013 and 0.0018, respectively, in close agreement with the specified values of z_{ow} and the ice values of Seifert and Langleben (1972) and Large and Pond (1981). The largest drag coefficient is approximately 0.0026 for ice concentrations between 50% and 60%. A similar result was obtained during the experiment REFLEX I by Hartmann *et al.* (1994), while Andreas et al. (1987) and Anderson (1987) estimate the maximum of C_d at about 80% ice concentration and Guest and Davidson (1987) do not find any distinct maximum. Since besides Hartmann *et al.* (1994) the other studies are based on less detailed surface information we feel rather confident that findings have a high degree of certainty.

The solid curve in Figure 6 is calculated taking into account the influence of floe edges and ice ridges while the dashed curve only reveals the influence of the floe edges. The increase of C_{dn} for ice concentrations from 0 to 0.5 is mainly caused by the increase of form drag of the ice floe edges. The decrease at higher ice concentrations reflects the smaller spacing of floes and the shadowing effect at the leeward side of the floes. This effect causes a substantial decrease of up to 15% of the total drag for ice concentrations above 20% and is maximum for $C = 100\%$. Investigations on the ratio $|F_f|/|S_{wo}|$ show a maximum of 1.0 at $C = 50\%$ and, as prescribed by the model, vanishing values close to $C = 0\%$ and 100%.

The results of this study are compared with the simpler model of Hartmann *et al.* (1994) assuming that the circumference of the floe is proportional to l_f and the area of the floe is proportional to l_f^2 . Under this assumption a relation of the form

$$\frac{|\vec{F}_f|}{|\vec{S}_{wo}|} \sim \frac{\bar{h}_f}{\bar{l}_f} C \tag{22}$$

should be valid.

This is confirmed by Figure 7 for the averaged quantities. The standard deviations reflect the shortcomings of their geometrical simplification for certain ice conditions.

Acknowledgements

We thank all our colleagues who helped perform the experiments during REFLEX II and Arktis 93. Dr. J. Hartmann, A. Borchert and W. Cohrs made important constributions to the data analysis. The authors wish to thank Prof. E. Augstein for his comments on the manuscript and the numerous discussions. The paper comprises AWI-contribution No. 892.

References

Anderson, R. J. : 1987, `Wind Stress Measurements Over Rough Ice During the 1984 Marginal Ice Zone Experiment´, *J. Geophys. Res.* **92**, 6933 – 6941.

Andreas, E. L., Tucker, W. B., and Ackley, S. F. : 1984, `Atmospheric Boundary-Layer Modification, Drag-Coefficient and Surface Heat Flux in the Antarctic Marginal Ice Zone ´, *J. Geophys. Res.* **89**, 649-661.

Arya, S. P.S. : 1973, `Contribution of Form Drag on Pressure Ridges to the Air Stress on Arctic Ice´, *J. Geophys. Res.* **30**, 7092-7099.

Arya, S. P.S. : 1975, `A Drag-Partition Theory for Determining the Large-Scale Roughness Parameter and Wind Stress on Artic Pack Ice´, *J. Geophys. Res.* **80**, 3447-3454.

Banke, E. G. and Smith, S. D. : 1973, `Wind Stress on Arctic Sea Ice´, *J. Geophys. Res.* **78**, 7871-7882.

Borchert, A. and Wamser, C. : 1994, ´New Airborne Line Scanner Systems for High Resolution Sea Ice Observations`, *The Global Atmosphere-Ocean System 2,* 247-251.

Dierking, W. : 1995, ´Laser Profiling of the Ice Surface Topography During the Winter Weddell Gyre Study 1992´, *J. Geophys. Res.* **100**, 4807-4820.

Gloersen, P. and Campbell, W. J. : 1988, ´Variations in the Arctic, Antarctic and Global Sea Ice Covers During 1978-1987 as Observed with Nimbus 7 Scanning Multichannel Microwave Radiometer´, *J. Geophys. Res.* **93**, 10666-10674.

Guest. P. S. and Davidson, K. L. : 1987, ´The Effect of Observed Ice Conditions on the Drag Coefficient In the Summer East Greenland Sea Marginal Ice Zone´, *J. Geophys. Res.* **92**, 6943-6954.

Hanssen-Bauer, I. and Gjessing, Y. T. : 1988, ´Observations and Model Calculations of Aerodynamic Drag on Sea Ice in the Fram Strait´, *Tellus*, **40A**, 151-161.

Hartmann, J., Kottmeier, C. and Wamser, C. : 1992, ´Radiation and Eddy Flux Experiment 1991 (Reflex I)´, *Reports on Polar Research,* **105**.

Hartmann, J., Kottmeier, C., Wamser, C. and Augstein, E. : 1994, ´Aircraft Measured Atmospheric Momentum, Heat and Radiation Fluxes Over Arctic Sea Ice, in the Polar Oceans and their Role in Shaping the Global Enviornment´, *Geophys. Monogr. Ser.* **85**, ed. O. M. Johannessen, R. D. Muench und J. E. Overland, 443-454, AGU, Washington.

Joffre, S. M. : 1983, ´Determining the Form Drag Contribution to the Total Stress of the Atmospheric Flow Over Ridged Sea Ice´, *J. Geophys. Res.* **88**, 4524-4530.

Kottmeier, Ch., Hartmann, J. ,Wamser, C. , Bochert, A., Lüpkes, C., Freese, D. and Cohrs, W. : 1994,´Radiation and Eddy Flux Experiment 1993 (Reflex II)´, *Reports on Polar Research,* **133**.

Large, W. G. and Pond, S. : 1981,´Open Ocean Momentum Flux Measurements in Moderate to Strong Winds´, *J. Phys. Oceanogr.* **11**, 324-336.

Mai, S. : 1995, ´Beziehungen zwischen Geometrischer und Aerodynamischer Oberflächenrauigkeit Arktischer Meereisflächen´, Diploma thesis in physics at the University of Bremen.

Marshall, J. K. : 1971, ´Drag Measurements in Roughness Arrays of Varying Density and Distribution´, *Agr. Meteorol.* **8**, 269-292.

Overland, J. E. : 1985, ´Atmospheric Boundary Layer Structure and Drag Coefficients Over Sea Ice´, *J. Geophys. Res.* **95**, 9029-9049.

Plate, E. J. and Lin, C. W. : 1965, ´ The Velocity Field Downstream from a Two-Dimensional Model Hill´, *Fluid Dynam. Diffus. Lab. Report No. CER65EJP14,* Colorado State University, Fort Collins, Colorado.

Raasch, S. : 1988, ´Numerische Simulation zur Entwicklung von Wirbelrollen und konvektiver Grenzschicht bei Kaltluftausbrüchen über dem Meer´, Ph. D thesis, University of Hannover.

Seifert, W. J. and Langleben, M. P. : 1972, ´Air Drag Coefficient and Roughness Length of a Cover of Sea Ice´, *J. Geophys. Res.* **77**, 2708-2713.

Wadhams, P. and Davy, T. : 1986, ´On The Spacing and Draft Distributions for Pressure Ridge Keels´, *J. Geophys. Res.* **91**(C9), 10697-10708.

Wefelmeier, C. and Etling, D. : 1991, ´The Influence of Sea Ice Distribution on the Atmospheric Boundary Layer´, *Z. Meteorol.* **41**, 333-342.